

Molecular Simulations Highlight the Role of Metals in Catalysis and Inhibition of Type II Topoisomerase

Giulia Palermo,^{†,‡} Marco Stenta,^{‡,§} Andrea Cavalli,^{†,§} Matteo Dal Peraro,^{*,‡} and Marco De Vivo^{*,†}

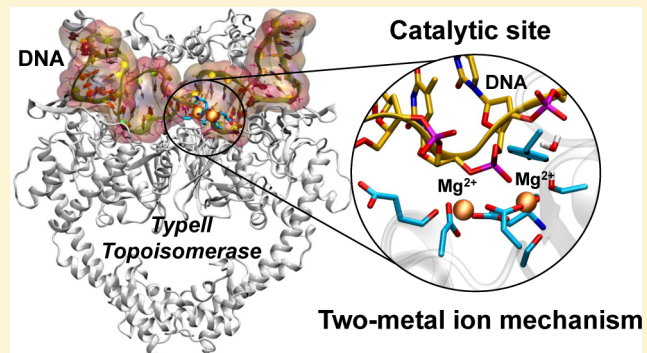
[†]Department of Drug Discovery and Development, Italian Institute of Technology, via Morego 30, 16163 Genova, Italy

[‡]Institute of Bioengineering, School of Life Sciences, Ecole Polytechnique Fédérale de Lausanne - EPFL, Lausanne, CH-1015, Switzerland

[§]Department of Pharmaceutical Sciences, University of Bologna, via Belmeloro 6, I-40126 Bologna, Italy

Supporting Information

ABSTRACT: Type II topoisomerase (topoII) is a metalloenzyme targeted by clinical antibiotics and anticancer agents. Here, we integrate existing structural data with molecular simulation and propose a model for the yet uncharacterized structure of the reactant state of topoII. This model describes a canonical two-metal-ion mechanism and suggests how the metals could rearrange at the catalytic pocket during enzymatic turnover, explaining also experimental evidence for topoII inhibition. These results call for further experimental validation.



Type II topoisomerase (topoII) is a metalloenzyme that controls the topology of DNA by cleaving and religating both strands of a DNA duplex. These transient breaks in the double helix are required to relax superhelical tension and knots during DNA strand separation in replication, transcription, recombination, and repair of the DNA.^{1,2} Therefore, topoII is a key target for clinical antibiotics (e.g., quinolones) and anticancer agents (e.g., anthracyclines).^{3–6} Despite the biological relevance of topoII enzymes and their established role as targets for drug discovery, the metal-aided mechanism for DNA cleavage and religation is still poorly understood.^{7,8}

TopoII cleaves and ligates DNA using active site tyrosine residues, which act as nucleophilic agents for the attack on the DNA backbone. The resulting transesterification reaction leads to the formation of a covalent phosphotyrosyl bond that links topoII and part of the DNA, which is therefore locked to topoII. This complex, referred to as a “cleavage complex” is then ligated back during the catalytic topoII cycle, regenerating the intact DNA chain. Over the past few years, a number of very informative X-ray structures of topoII have been resolved, with either one or two divalent ions in the catalytic site. Also, drugs such as the anticancer etoposide or quinolones, a major class of antibiotics, have been shown to bind the cleavage complex, blocking the topoII religation step.^{3,7,9–16} However, the experimental conditions used to obtain those crystals, such as the presence of an intercalated topoII inhibitor—which can critically affect the disposition of catalytic groups within the complex—and/or active site tyrosine mutation, and/or the use of noncatalytic metal ions, have so far precluded the resolution of the topoII reactant state, which is needed to understand the

reaction mechanism for catalysis. Only one available X-ray structure reports a drug-free resealed DNA complex, obtained via drug back-soaking, which shows only one single Mg²⁺ ion in the catalytic site.¹⁵

The X-ray structures of topoII containing only one metal ion in the catalytic site initially led to the hypothesis that the catalytic reaction could be aided by a single “dynamic” Mg²⁺ ion, which would move between two metal binding sites in the catalytic pocket of topoII. More recently, however, structural data on the yeast topoII–DNA cleavage complex detected two ions in a nonclassical coordination in the active site, suggesting a novel two-metal-ion mechanism for topoII catalysis.¹⁶ In this structure, only one metal (metal A, Me_A) seems to have an active role in catalysis promoting the exit of the leaving group, while the second ion (metal B, Me_B) is proposed to have only a structural role in anchoring the substrate DNA during catalysis. This was described as a variation of the canonical two-metal-ion mechanism originally proposed by Steitz and Steitz,¹⁷ in which both metals are coordinated to the scissile phosphate and actively participate in the enzymatic reaction. It is worth reminding that, in the yeast topoII structure,¹⁶ the nucleophilic Y782 is bound to a nicked DNA. In addition, other factors, such as the unnatural 3'-bridging phosphorothiolate that caps the remaining DNA strand and the use of zinc for crystal soaking, were used to obtain the X-ray structure.¹⁶ Zinc is not catalytically relevant for topoII and is known to have a different coordination geometry with respect to magnesium, natively

Received: August 6, 2012

Published: January 9, 2013

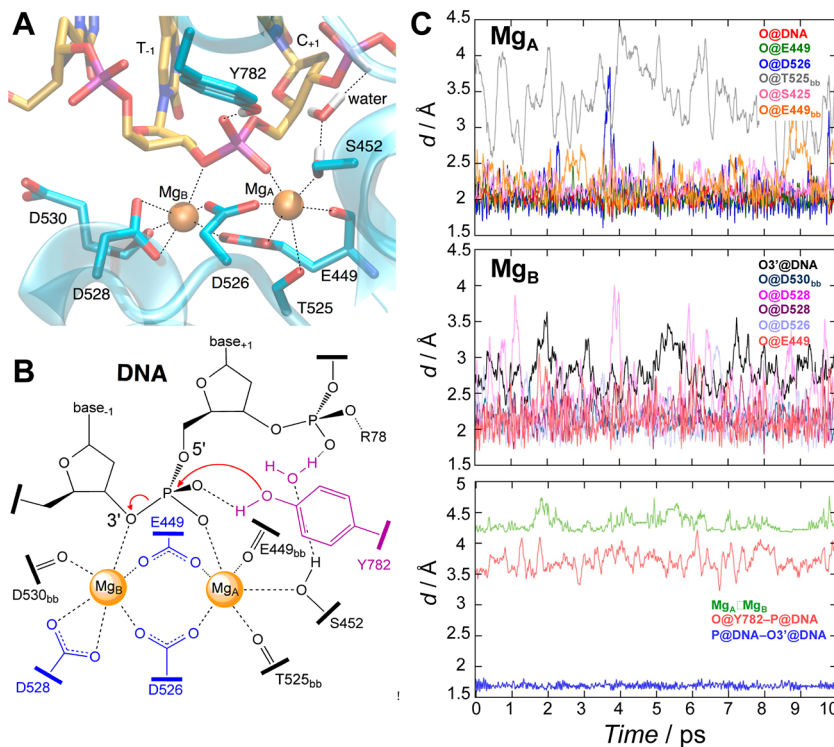


Figure 1. (A) Type II topoisomerase–DNA complex, *S. cerevisiae* topoII active site equilibrated by >20 ns of classical MD and by >10 ps of DFT-based QM/MM MD (noninteracting hydrogens are removed for clarity). (B) Canonical-like two-metal-ion mechanism proposed for topoII as emerged from classical and QM/MM calculations on the yeast topoII X-ray structure.¹⁶ The conserved two-metal-ion DDE motif is indicated by blue residues, while the purple are indicative of groups likely to be involved in the reaction. (C) Structural properties from *ab initio* QM/MM-MD of Enz-R. Time evolution of the coordination distances (d) for Mg_A (upper graph) and Mg_B (central graph) and forming/breaking bonds (lower graph). In the lower graph, the forming bond (O@Y782–P@DNA), the breaking bond (P@DNA–O3'@DNA), and the interionic distance (Mg_A–Mg_B) are reported. Distances are in Å.

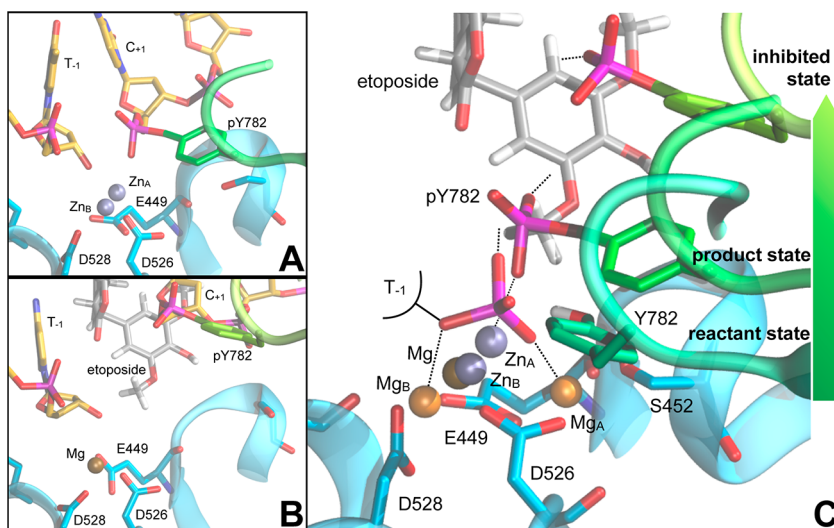


Figure 2. (A) Type II topoisomerase–DNA complex, as reported in ref 16. (B) X-ray structure of the human Topo2b complexed to DNA and to the anticancer drug etoposide.⁹ (C) Superimposition of our model (reactant state, Figure 1A), the Zn²⁺-complexed X-ray structure (as shown in A) and the product inhibited state complexed with etoposide (as shown in B). Y782 is in green, from darker to lighter, to indicate its gradual shift and rotation from the reactant state, to product and, eventually, inhibited state (green arrow on the right).

used by the enzyme. Altogether, these conditions might have perturbed the optimal reactants' conformation of metals at the active site, shifting the topoII conformation closer to the product state of the DNA cleavage complex. Therefore, in light of these structural data,¹⁶ we decided to model the arrangement of the two Mg²⁺ ions in the reactants state, a conformation not

experimentally characterized yet. We investigated whether the two metals can reorganize their position and coordination shell during catalysis, as observed in other enzymes using the two-metal-ion mechanism.¹⁸

Characterization of the Catalytically Competent State of topoII Using Classical MD

Using the available structure

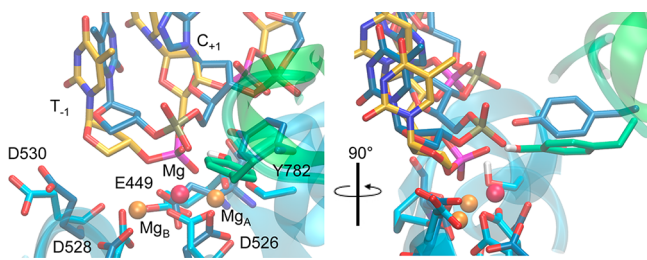


Figure 3. Superimposition of our model (reactant state, Figure 1A) and the drug-free resealed DNA complex reported in ref 15, which shows a single Mg^{2+} ion (Mg^{2+} is the violet sphere, while carbon atoms are in blue). Here, it is shown how two Mg^{2+} ions complete their octahedral coordination shells, compared to the structure having a single Mg^{2+} ion. The right panel shows the same superimposition with a rotation of 90° on the perpendicular axis. This allows showing better how the single Mg^{2+} ion coordinates the scissile phosphate, being however positioned above the plane of the two Mg^{2+} ions (Mg_A and Mg_B). Mg is located in between Mg_A and Mg_B , being partially coordinated only to D526 and E449.

in complex with two zinc ions (PDB code 3L4K), solved at 2.98 \AA resolution,¹⁶ we reconstructed the topoII–DNA Michaelis complex in a catalytically competent state, detaching the DNA substrate from the nucleophilic Y782, while the natural O3'–P bond was reconstituted. The two noncatalytic Zn^{2+} metals observed in the crystal were replaced by Mg^{2+} ions. The obtained system was then solvated in water at physiological $MgCl_2$ concentration ($\sim 10\text{ mM}$). This model, hereafter referred to as *Enz-R*, was equilibrated with classical molecular dynamics¹⁹ (MD) at 298 K and 1 atm for more than $\sim 20\text{ ns}$, adopting a simulation protocol applied to other phosphodiesterases.^{20,21}

The product state, i.e., the so-called “DNA cleavage complex,” hereafter referred to as *Enz-P*, was also subjected to classical MD simulations to understand its structural features. Classical MD simulations of the original X-ray structure containing Zn^{2+} –*Enz-P/X-ray*—were carried out and compared with the *Enz-P* system.²²

In *Enz-R*, in less than $\sim 1\text{ ns}$ the active site spontaneously relaxed into a canonical-like two-metal-ion architecture,¹⁷ which was maintained throughout the classical MD simulations. In detail, Mg_A and Mg_B shifted concertedly by $\sim 3.3\text{ \AA}$, with the saturation of their octahedral coordination shells using surrounding acidic residues and the scissile phosphate (Figure 1A). In our structure, Mg_A coordinates the scissile phosphate and T525 backbone in apical positions, whereas the Mg_A basal plane ligands are D526, E449 (with its backbone and side-chain), and S452. Mg_B coordinates the 3'-OH leaving group and D528 in apical positions, whereas D530 (backbone), E449, D526, and D528 saturate its basal coordination plane. In this conformation, the Mg_A coordination sphere is arranged to optimally locate Y782 for the nucleophilic attack on the phosphate (3.6 \AA distance, Figure 1B). Most of the features of the initial X-ray structure were preserved in the final model. In particular, the root-mean-square deviation (RMSD) of the protein was as low as $2.6 \pm 0.1\text{ \AA}$, and $3.2 \pm 0.3\text{ \AA}$ for the DNA strands (Figure S2).

In *Enz-P* and *Enz-P/X-ray*, the coordination of the two metal ions, as in the X-ray structure reported by Schmidt et al.,¹⁶ is well maintained during classical MD (Figures S4, S5, and S6). Additional water molecules complete the octahedral (Mg^{2+}) and tetrahedral (Zn^{2+}) coordination spheres of the metals in *Enz-P* and *Enz-P/X-ray*, respectively (see the Supporting

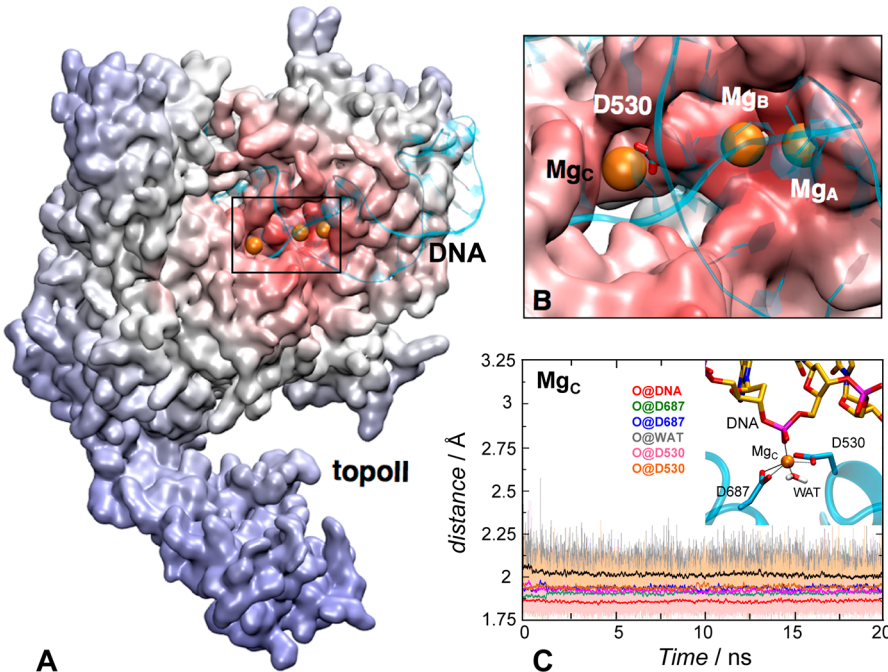


Figure 4. Electrostatic properties at the metal pocket in *Enz-R*. (A) The electrostatic potential (accounting for the topoII–DNA complex solvated in water) is explicitly calculated from the MD trajectory and mapped onto the molecular surface of one monomer of the topoII dimeric complex. Only one monomer of topoII is shown, and the DNA strands are depicted in ribbon representation, while the Mg^{2+} metals are depicted as orange vdW spheres. The color scale goes from red (-1000 in units of kT/e [J/C]) to blue ($+400$ kT/e [J/C]), highlighting the negatively charged channel connecting the catalytic site and the bulk. (B) Focus on the catalytic site of topoII; D530 is also shown in licorice representation as the main ligands coordinating the third Mg^{2+} metal (Mg_C) observed at the catalytic pocket. (C) Time evolution of the coordination distances for Mg_C during classical MD of the *Enz-R* system. The Mg_C coordination sphere is shown on the right top of the graph. Distances are in \AA .

Information, SI). As a result, the position of the metal ions is different in the reactant (i.e., canonical-like)²³ and product (i.e., non canonical-like)¹⁶ states, leading to the hypothesis of a gradual shift of the two metals from the reactants to the products, which was not ruled out by Schmidt et al.¹⁶ In fact, in the canonical two-metal aided phosphoryl transfer reaction, the two metals act cooperatively during the catalysis, facilitating nucleophile formation and stabilizing both transition state and leaving group.^{20,23,24} This seems to be the mechanism suggested by the reactant state in our system, which is characterized by a canonical-like two-metal-ion architecture (Figure 1A) that would catalyze efficiently the enzymatic reaction.

Reactants State Refinement Using QM/MM Simulations. A selected MD snapshot of the *Enz-R* system was optimized at the quantum mechanics/molecular mechanics (QM/MM) level, using the COBRAMM software package.²⁵ The Amber ff99SB^{26,27} parameters were used to describe the MM part, while the QM region (112 atoms in total, including Mg_A and Mg_B; the S452, T525, D528, D530, E449, G450, Y782 residues; one water molecule; and key atoms of the nucleic acid involved in the reaction, Figure S1) was treated at the density functional theory (DFT) level using the B3LYP^{28–30} functional and the def2-SV(P) basis set.³¹ Then, the optimized structure of *Enz-R* was further refined by means of QM/MM-MD simulations, maintaining the same QM/MM partition of the system. The simulation was carried out with the program CP2K,^{32–34} in the Born–Oppenheimer approximation in the canonical (NVT) ensemble. The QM region was treated at the DFT/BLYP³⁵ level.³⁶ Initially, the system was equilibrated for ~4 ps, keeping fixed the heavy atoms of the QM part. Then, ~14 ps of unrestrained molecular dynamics were carried out. Structural analyses were performed on the equilibrated system, on the last ~10 ps of dynamics.

DFT-based QM/MM optimizations and over 10 ps of QM/MM-MD confirmed the two Mg²⁺ ions' rearrangement in *Enz-R*, which is characterized by a canonical-like two-metal-ion architecture of the active site (Figure 1). After superimposition of the optimized structure onto the Zn²⁺-based X-ray reference structure,¹⁶ the catalytic site RMSD was ~1.5 Å (Figure 2C). During QM/MM dynamics, Mg_A stably coordinates the scissile phosphate at 2.03 ± 0.09 Å and its basal plane ligand D526 at 2.09 ± 0.26 Å (Figure 1C). The residue E449 is bound to Mg_A with its backbone at 2.23 ± 0.26 Å and side chain at 2.04 ± 0.13 Å. To complete the octahedral coordination shell, Mg_A binds S452 at 2.21 ± 0.13 Å and the T525 backbone in the apical position at 3.39 ± 0.44 Å. Mg_B coordinates the 3'-OH leaving group at 2.80 ± 0.25 Å and the two D528 side-chain oxygens at 2.49 ± 0.40 Å and 2.17 ± 0.17 Å, respectively. E449 remains at 2.16 ± 0.24 Å from Mg_B, whereas D530 (backbone) and D526 saturate the Mg_B basal coordination plane at 2.14 ± 0.12 Å and 2.13 ± 0.25 Å, respectively. In this conformation, the Mg_A coordination sphere is arranged to optimally locate Y782 for the nucleophilic attack on the phosphate (3.71 ± 0.15 Å distance, Figure 1C). Moreover, the interionic Mg_A–Mg_B distance remains stable during QM/MM dynamics and is on average 4.32 ± 0.11 Å.

Structural Determinants Supporting a Canonical Two-Metal Ion Mechanism. Interestingly, the DNA cleavage mechanism can be favored by R781 and one ordered water molecule, which H-bonds to S452 and the C₋₁ phosphate (Figure 1A).¹⁶ In particular, during the classical MD simulations of *Enz-R*, R781 remains within ~4 Å from the

nucleophilic Y782, being also next to the scissile phosphate. This supports the proposed role of R781 in aiding the DNA cleavage by lowering the pK_a of the attacking Y782.^{16,37,38} In *Enz-P*, R781 moves slightly away from the catalytic center. This would indicate that, in the products state, R781 slides aside to allow DNA opening and, later, likely help in the religation of the DNA double strand (see SI). On the other side of the cleavage center, Mg_B mostly stabilizes the 3'-OH leaving group, as in the canonical two-metal-ion motif. In this way, both metals can concur to the catalytic reaction mechanism stabilizing concertedly the nucleophilic tyrosine, the leaving group, and the scissile phosphate during phosphodiester bond cleavage, as shown for other phosphodiesterases.^{20,39} In this dynamic model, we also observed that additional water molecules can freely access the catalytic site and, H-bonding to Y782, likely promote proton transfer events required during the reaction (Figure 1 and SI).²⁰

In our model, the competent reactant state is promoted by the recruitment in the active pocket of two Mg²⁺ ions that can be accommodated into a canonical two-metal-ion motif, favoring the nucleophilic attack of Y782. Once the 5'-phosphotyrosine is formed, the metal ions partially abandon their coordination and rearrange into the pocket, assuming a conformation likely similar to that trapped in the X-ray structure recently reported (Figure 2A,C). The net result is that the DNA cleavage is producing a large movement of the 5'-phosphotyrosine at the catalytic pocket, which is dragging out one metal ion (Me_A), still partially coordinated with the scissile phosphate. The other metal (Me_B) is not able to hold the initial coordination with the leaving phosphate, remaining in the pocket (Figure 2A,C). Interestingly, classical MD simulations of the DNA cleavage complex confirmed that the two metals (Mg²⁺) conserved a position similar to the crystallographic structure complexed with Zn²⁺, with minor rearrangements of the metal ions and surrounding ligands (Figure S4). Therefore, we found a precatalytic state of the topoII–DNA complex showing a canonical-like two-metal-ion motif of the active site,¹⁷ which differs from the starting Zn²⁺-complexed X-ray structure.¹⁶ The overlap of the two-metal-ion model with the only X-ray structure having a drug-free resealed DNA complex¹⁵ shows how the second Mg²⁺ ion disposes itself within the catalytic pocket, allowing octahedral coordination shells of the two Mg²⁺ ions, using surrounding acidic residues and the scissile phosphate (Figure 3). While our computationally refined structural model clearly needs experimental validation, it provides an intriguing and computationally robust indication that topoII could function through the two-metal-ion mechanism, as several other two-metal-ion phosphodiesterases.¹⁸

Metal Ions Displacement for TopoII Inhibition. The functional arrangement of metal ions observed here to modulate the topoisomerase reaction can also explain new aspects of topoII inhibition. In fact, a recent crystal structure of topoII in complex with the anticancer drug etoposide⁹ clearly indicates a large opening of the catalytic site, caused first by DNA cleavage and then by etoposide insertion into the DNA cleavage complex. From the structural superimposition of our model with the Zn²⁺-complexed X-ray structure (likely representing a product-like conformation) and with the inhibited product state complexed with etoposide, the gradual shift and rotation of the nucleophilic Y782, which moves further away from the catalytic site after the formation of the 5'-phosphotyrosine bond (see Figure 2C), is evident. The position

of the metal ions is different in the three structures—as highlighted in Figure 2C—as the 5'-phosphotyrosine pulls out part of the cleaved DNA from the catalytic site. In the product-like state, one Zn^{2+} ion (Zn_B) overlaps almost perfectly with the only Mg^{2+} ion present in the etoposide's structure. This might be caused by the 3'-methoxyl group of etoposide, which points directly into the metal coordination sphere and displaces one metal ion, therefore producing a large perturbation in the two-metal-ion motif of the catalytic site. Most likely, this explains why etoposide activity is sensibly reduced if the 3'- or 5'-methoxyl groups are replaced with smaller atoms, such as hydrogens.⁴⁰

Possible Role of a Third Metal Ion in Catalysis. Another interesting observation from our simulations on the dynamic rearrangement of metal ions at the topoII active pocket regards the conserved D530 residue, which could play a role in recruiting metals to populate the active site upon catalytic turnover. In fact, the salt-bridge D530–R690, present in the X-ray structure, is broken during the MD simulations of the reactant state in favor of Mg^{2+} ions freely accessing the active site pocket, thanks to a negatively charged channel connecting from the bulk (Figure 4). In particular, D530 is found to coordinate a stable third Mg^{2+} ion (namely Mg_C , Figure S9) ~10 Å away from Mg_B , in both the reactant and product states. This suggests that this second-shell acidic ligand might modulate cation uptake and release at the active site upon DNA cleavage complex formation, similarly to what recently proposed for RNase H.²¹ Furthermore, as suggested also by the X-ray data,¹⁶ the observed flexibility of the metal coordination sphere may be functional to the stabilization of different states along the DNA cleavage/religation reaction.⁴¹

In conclusion, our study reports a quantum mechanics-based model of the structure of the competent reactants state of topoII in complex with DNA under native catalytic conditions, which is still experimentally unrevealed. On the basis of our findings, we propose this state to be characterized by an active site architecture reminiscent of the canonical two-metal-ion mechanism.¹⁷ Our model agrees with what was seen in several other phosphodiesterases,¹⁸ suggesting that the two-metal-ion mechanism is structurally reasonable for topoII, as well, with both metals involved actively in the catalytic reaction. Interpreted with existing metal-complexed structures of topoII in which the 5'-phosphotyrosine is formed, our model can also rationalize experimental findings on topoII inhibition, through a possible dynamic rearrangement of the metal ions in an extended neighborhood of the catalytic pocket. In light of the overall evidence we discussed above, we therefore hypothesize that topoII can function through the two-metal-ion mechanism. We hope that these results will now stimulate further experimental studies to reach a consensus on the metal coordination in the reactant state of topoII.

ASSOCIATED CONTENT

Supporting Information

Additional information on materials and methods and results. This material is available free of charge via the Internet at <http://pubs.acs.org>.

AUTHOR INFORMATION

Corresponding Author

*E-mail: marco.devivo@iit.it (M.D.V.), matteo.dalperaro@epfl.ch (M.D.P.).

Author Contributions

#Equally contributed

Notes

The authors declare no competing financial interest.

ACKNOWLEDGMENTS

The authors thank the IIT Platform “Computation” for CPU time. This work was supported by a grant from the Swiss National Supercomputing Centre (CSCS) under project ID 8330.

REFERENCES

- (1) Sissi, C.; Palumbo, M. *Cell. Mol. Life Sci.* **2011**, *67*, 2001–2024.
- (2) Yang, W. *Q. Rev. Biophys.* **2011**, *44*, 1–93.
- (3) Bax, B. D.; Chan, P. F.; Eggleston, D. S.; Fosberry, A.; Gentry, D. R.; Gorrec, F.; Giordano, I.; Hann, M. M.; Hennessy, A.; Hibbs, M.; Huang, J.; Jones, E.; Jones, J.; Brown, K. K.; Lewis, C. J.; May, E. W.; Saunders, M. R.; Singh, O.; Spitzfaden, C. E.; Shen, C.; Shillings, A.; Theobald, A. J.; Wohlkonig, A.; Pearson, N. D.; Gwynn, M. N. *Nature* **2010**, *466*, 935–940.
- (4) Bailly, C. *Chem. Rev.* **2012**, *112*, 3611–3640.
- (5) Pommier, Y.; Leo, E.; Zhang, H.; Marchand, C. *Chem. Biol.* **2010**, *17*, 421–433.
- (6) The antibacterial lead discovery challenge. *Nat. Rev. Drug Discovery* **2010**, *9*, 751–752.
- (7) Sissi, C.; Palumbo, M. *Nucleic Acids Res.* **2009**, *37*, 702–711.
- (8) Deweese, J. E.; Osheroff, N. *Nucleic Acids Res.* **2009**, *37*, 738–748.
- (9) Wu, C. C.; Li, T. K.; Farh, L.; Lin, L. Y.; Lin, T. S.; Yu, Y. J.; Yen, T. J.; Chiang, C. W.; Chan, N. L. *Science* **2011**, *333*, 459–462.
- (10) Wohlkonig, A.; Chan, P. F.; Fosberry, A. P.; Homes, P.; Huang, J.; Kranz, M.; Leydon, V. R.; Miles, T. J.; Pearson, N. D.; Perera, R. L.; Shillings, A. J.; Gwynn, M. N.; Bax, B. D. *Nat. Struct. Mol. Biol.* **2010**, *17*, 1152–1153.
- (11) Dupureur, C. M. *Metallomics* **2010**, *2*, 609–620.
- (12) Laponogov, I.; Sohi, M. K.; Veselkov, D. A.; Pan, X. S.; Sawhney, R.; Thompson, A. W.; McAuley, K. E.; Fisher, L. M.; Sanderson, M. R. *Nat. Struct. Mol. Biol.* **2009**, *16*, 667–669.
- (13) Pitts, S. L.; Liou, G. F.; Mitchenall, L. A.; Burgin, A. B.; Maxwell, A.; Neuman, K. C.; Osheroff, N. *Nucleic Acids Res.* **2011**, *39*, 4808–4817.
- (14) Deweese, J. E.; Osheroff, N. *Metallomics* **2010**, *2*, 450–459.
- (15) Laponogov, I.; Pan, X. S.; Veselkov, D. A.; McAuley, K. E.; Fisher, L. M.; Sanderson, M. R. *PLoS One* **2010**, *5*, e11338.
- (16) Schmidt, B. H.; Burgin, A. B.; Deweese, J. E.; Osheroff, N.; Berger, J. M. *Nature* **2010**, *465*, 641–644.
- (17) Steitz, T. A.; Steitz, J. A. *Proc. Natl. Acad. Sci. U. S. A.* **1993**, *90*, 6498–6502.
- (18) Yang, W.; Lee, J. Y.; Nowotny, M. *Mol. Cell* **2006**, *22*, 5–13.
- (19) Lindorff-Larsen, K.; Piana, S.; Palmo, K.; Maragakis, P.; Klepeis, J. L.; Dror, R. O.; Shaw, D. E. *Proteins* **2008**, *78*, 1950–1958.
- (20) De Vivo, M.; Dal Peraro, M.; Klein, M. L. *J. Am. Chem. Soc.* **2008**, *130*, 10955–10962.
- (21) Ho, M. H.; De Vivo, M.; Dal Peraro, M.; Klein, M. L. *J. Am. Chem. Soc.* **2010**, *132*, 13702–13712.
- (22) Force-field parameters for the metal ions [(a) Aqvist, J. *J. Phys. Chem.* **1990**, *94*, 8021–8024. (b) Pang, Y. P. *J. Mol. Model.* **1999**, *5*, 196–202] here employed allowed an octahedral (Mg^{2+}) and tetrahedral (Zn^{2+}) coordination sphere for the metals within the topoII active site. Full details are reported in the SI, sections 1.2 and 2.3.
- (23) Steitz, T. A.; Steitz, J. A. *Proc. Natl. Acad. Sci. U. S. A.* **1993**, *90*, 6498–6502.
- (24) Yang, W.; Lee, J. Y.; Nowotny, M. *Mol. Cell* **2006**, *22*, 5–13.
- (25) Altoè, P.; Stenta, M.; Bottani, A.; Garavelli, G. *Theor. Chem. Acc.* **2007**, *118*, 219–240.

- (26) Hornak, V.; Abel, R.; Okur, A.; Strockbine, B.; Roitberg, A.; Simmerling, C. *Proteins* **2006**, *65*, 712–715.
- (27) Ponder, J. W.; Case, D. A. *Adv. Protein Chem.* **2003**, *66*, 27–85.
- (28) Becke, A. D. *J. Chem. Phys.* **1993**, *98*, 1372–1377.
- (29) Kim, K.; Jordan, K. D. *J. Phys. Chem.* **1994**, *98*, 10089–10094.
- (30) Stephens, P. J.; Devlin, C. F.; Chabalowski, C. F.; Frisch, M. J. *J. Phys. Chem.* **1994**, *98*, 11623–11627.
- (31) Schaefer, A.; Horn, H.; Ahlrichs, R. *J. Chem. Phys.* **1992**, *97*, 2571–2577.
- (32) Laino, T.; Mohamed, F.; Laio, A.; Parrinello, M. *J. Chem. Theory Comput.* **2005**, *1*, 1176–1184.
- (33) VandeVondele, J.; Krack, M.; Mohamed, F.; Parrinello, M.; Chassaing, T.; Hutter, J. *Comput. Phys. Commun.* **2005**, *167*, 103–128.
- (34) Freely available at the URL <http://cp2k.berlios.de>, released under GPL license.
- (35) Lee, C. T.; Yang, W. T.; Parr, R. G. *Phys. Rev. B* **1988**, *37*, 785–789.
- (36) A double- ζ DZVP valence basis set (for H, C, N, O, P atoms) and a triple- ζ TZVD valence basis set (for Mg²⁺ atoms) were employed in conjunction with auxiliary plane-wave basis set (with a density cutoff of 280 Ry). The Goedecker-Teter-Hutter (GTH) pseudopotentials were used to describe the core electrons [(a) Goedecker, S.; Teter, M.; Hutter, J. *Phys. Rev. B* **1996**, *54*, 1703–1710. (b) Hartwigsen, C.; Goedecker, S.; Hutter, J. *Phys. Rev. B* **1998**, *58*, 3641–3662]. The remaining part of the system, including water molecules and counterions, was treated at the classical level with the Amber ff99SB. The valence of the terminal QM atoms was saturated by the addition of capping hydrogen atoms. An integration time step of 0.5 ps was used. The Bussi thermostat [(c) Bussi, G.; Donadio, D.; Parrinello, M. *J. Chem. Phys.* **2007**, *126*, 014101] was adopted to keep the temperature of the system at 300 K. Full details are reported in the SI, section 1.3.
- (37) Liu, Q.; Wang, J. C. *J. Biol. Chem.* **1998**, *273*, 20252–20260.
- (38) Okada, Y.; Ito, Y.; Kikuchi, A.; Nimura, Y.; Yoshida, S.; Suzuki, M. *J. Biol. Chem.* **2000**, *275*, 24630–24638.
- (39) Nowotny, M.; Yang, W. *EMBO J.* **2006**, *25*, 1924–1933.
- (40) Bender, R. P.; Jablonksy, M. J.; Shadid, M.; Romaine, I.; Dunlap, N.; Anklin, C.; Graves, D. E.; Osheroff, N. *Biochemistry* **2008**, *47*, 4501–4509.
- (41) Nakamura, T.; Zhao, Y.; Yamagata, Y.; Hua, Y. J.; Yang, W. *Nature* **2012**, *487*, 196–201.